18th International Conference
ENGINEERING MECHANICS 2012
Svratka, Czech Republic, May 14 – 17, 2012

pp. 1485–1491
Paper #282

X-RAY OBSERVATION OF THE LOADED SILICATE COMPOSITE

D. Vavřík[1], T. Fíla[2], I. Jandejsek[3], V. Veselý[4],

Abstract: *An intensive internal material damage evolution precedes a failure in quasi-brittle materials. Not only the existence of damage but also its quantification and the geometry of the Fracture Process Zone have to be identified in order to validate approaches on both numerical modelling of quasi-brittle behaviour and experimental determination of fracture properties. Radiographic techniques and Digital Image Correlation method are very appropriate for analysing of the Fracture Process Zone evolution during specimen loading.*

Keywords: ***Quasi-brittle fracture, Cementitious composite, Digital radiography, Computed tomography, Digital Image Correlation***

1. Introduction

The area of determination of characteristics of quasi-brittle building materials (most commonly cementitious composites) which should describe their ability to resist the fracture propagation has been thoroughly researched for several decades (van Mier, 1997, Bažant & Planas, 1998). However, some aspects that can be referred to as crucial are still among the topics of intensive research. Effects of the size and geometry of the test specimen (Yu et al., 2010) regarded also as the effect of the specimen free boundaries (Hu & Duan, 2007) seems to be the most relevant. An approach incorporating the parameters of the zone of material failure developing at the propagating macroscopic crack tip (fracture process zone, FPZ) has been proposed and (partially) employed recently (Veselý et al., 2009). The development of this approach is motivated by capturing of the above-mentioned effects in order to provide values of the fracture-mechanical parameters of the tested material independent of these effects. This methodology works with the reconstruction of the current size and shape of the FPZ (and perhaps also the intensity of the cohesive behaviour over the FPZ volume) (Veselý & Frantík, 2010) to which the amount of energy dissipated during the current step of fracture process should be related.

The development of the methodology is in a stage of testing, verification by numerical simulations (Frantík et al., 2011) and experimental validation (Vesely et al., 2010) at present. It has to be emphasized that sound experimental evidence the FPZ size and shape (and possibly other characteristics) is published rather rarely. Techniques based on acoustic emission (Otsuka & Date, 2000, Mihashi & Nomura, 1996, Muralidhara et al. 2010), holographic interferometry, X-ray imaging (in combination with digital image analysis − Jandejsek et. al. 2011) and infrared thermography were reported to be used to determine the FPZ in quasi-brittle materials (summarized e.g. in van Mier, 1997).

Investigation of the material failure employing X-ray imaging is presented in this paper. Notched specimen prepared from cementitious composite was loaded in three point bending in a specially designed loading device. Crack and FPZ shape was analysed using digital transmission radiography

[1] Ing. Daniel Vavřík, Ph.D.: Institute of Theoretical and Applied Mechanics AS CR v. v. i., Prosecka 76, Prague 9, Czech Republic, vavrik@itam.cas.cz, Institute of Experimental and Applied Physics, Czech Technical University in Prague, Horska 3a/22, Prague 2, Czech Republic

[2] Bc. Tomáš Fíla: Institute of Theoretical and Applied Mechanics AS CR v. v. i., Prosecka 76, Prague 9, Czech Republic, fila@itam.cas.cz

[3] Ing. Ivan Jandejsek: Institute of Theoretical and Applied Mechanics AS CR v. v. i., Prosecka 76, Prague 9, Czech Republic, jandejs@itam.cas.cz

[4] Ing. Václav Veselý, Ph.D.: Brno University of Technology, Faculty of Civil Engineering, Institute of Structural Mechanics, Veveří 331/95; 602 00, Brno; Czech Republic, vesely.v1@fce.vutbr.cz,

and X-ray Computed Tomography (XCT). Visualization of the FPZ was emphasized using tools of the Digital Image Correlation method (DIC).

2. Investigated material, specimen dimensions

The radiographic investigations of the material failure have limits in the dimensions of the test specimens. In our case, the length of the beam subjected to three point bending is limited by the chamber diameter of the loading device in which the specimen was placed.

As a material for the specimen preparation, a fine-grained cementitious composite was chosen to simulate the failure process of normal-sized building structures/structural members made of concrete. Commercial dry plaster mix with maximum aggregate size equal to 1.2 mm (limestone debris) was selected. The bonding agent of this mix consists of both cement and calcium hydroxide. Minimal value of modulus of rupture quoted by the producer is 0.7 MPa. The mix was prepared according to the producer's instructions.

The presented experiment was made as a pilot test to develop appropriate methodology of the FPZ and crack analysis intended for future experimental campaign. Series of 9 specimens were casted into the mould for this campaign. Three specimens' breadths B (15, 25 and 30 mm) were selected; three different notch lengths a (4, 10 and 16 mm) were taken into account for each specimen breadth B. The notches were cut using diamond saw. It provides the relative notch length α equal to 0.1, 0.25 and 0.4. Specimen height W and length L are equal to 40 and 150 mm, respectively. From this specimen series the specimen with 25 mm breadth and 10 mm notch length was selected for the developing of the methodology for macroscopic crack and FPZ analysis. The loading span of the specimen was set as equal to 120 mm. Schematic picture of the specimen and related bending test is depicted in Figure 1.

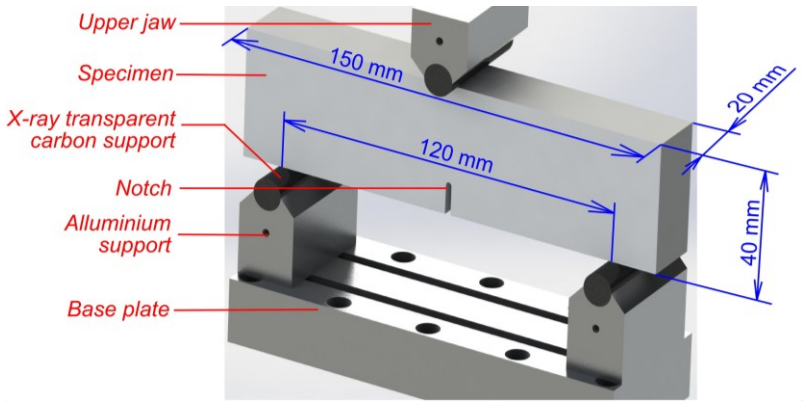

Figure 1: Three point bending of the specimen.

3. Instrumentation

The modular tomographic system (Jakůbek et. al., 2006) provides an experimental setup allowing positioning adjustment of the X-ray tube, motorized positioning of the detector and the operational movement of the observed object fixed on a motorized stage. The linear axis of this stage enables to set the projective magnification of the object. The rotation axis is used for tomographic data acquisition. The setup is equipped by the motorized revolver holder of the filters used for the fully automated acquisition of data needed for beam hardening correction, using the Signal to Equivalent Thickness (SET) method (Vavřík 2011).

Hamamatsu microspot tube is employed as X-ray source in the tomographic system. This tube has a 5 μm spot size and cone beam. The pixelated Hamamatsu flat panel was utilized as X-ray imager in our work. This detector has active area 120x120 mm with 50 μm pixel size. Binning of 2×2 pixels was used in our work, so effective pixel pitch was equal to 0.1 mm.

Highly stiff loading compressive device was used for the specimen loading. This device allows very low loading velocity while it's relatively low weight and dimensions enable X-ray observation of the specimen in the radiographic cabin. Loading device generally consists of the actuating part and of

the chamber in which specimen is placed. This chamber was manufactured from two parts. Top one is from the aluminium alloy and bottom one from the 0.6 mm thick carbon epoxy laminate, which is practically transparent for X-rays. These parts are connected using bayonet mechanism. Support pins of the bending mechanism were also prepared from the carbon material. This solution enables radiographic observation of the analysed specimen without any influence of the loading device for X-ray measurement. Whole setup is depicted in Figure 2 left. Disassembled chamber with the specimen is in Figure 2 right.

Figure 2: Radiographic setup with loading device left. Disassembled chamber with the specimen right.

4. Experimental details

Specimen was loaded with velocity 6 μm/min. Exposure time of one X-ray radiograms was 5×0.48 seconds (it corresponds to the 0.5 μm displacement increment due to read out time). These radiograms were recorded continuously during loading while CT measurement was done in two loading levels. For the CT measurement, 240 snapshots (180° rotation) were taken. Total time of one CT measurement was 50 minutes. The specimen rotation axis was at a distance 188 mm from the X-ray tube spot and flat panel was at distance 429 mm X-ray from the tube spot. The projected magnification was 2.3 from this reason. The X-ray tube was operated at 80 kV and 125 μA. CT reconstruction was done considering divergent X-ray beam (Vavřík & Soukup, 2011).

5. Results

A load−displacement diagram (LD diagram) is plotted in Figure 3. It is clearly visible that loading device enables to study processes with very high loading precision. The radiogram of the specimen taken 1.5 μm after reaching maximal loading force (point *A* in LD diagram: 108 N at 134 μm) is in Figure 4 left. Significant structure corresponds to the material inhomogeneity. It is almost impossible to observe FPZ directly in the investigated specimen thanks to this structure.

DIC tools were used to avoid this difficulty, where actual and initial radiograms were subtracted (subtraction image) to find changes of the specimen density considering specimen movement during its loading. Such image is shown in Figure 4 right (three blue diamond shape spots occurred thanks to flat panel local noise). It is visible that FPZ has significant role for the fracture mechanics description, where crack is much shorter (0.7 mm) than FPZ (6.5 mm) as visible in Figure 4 right.

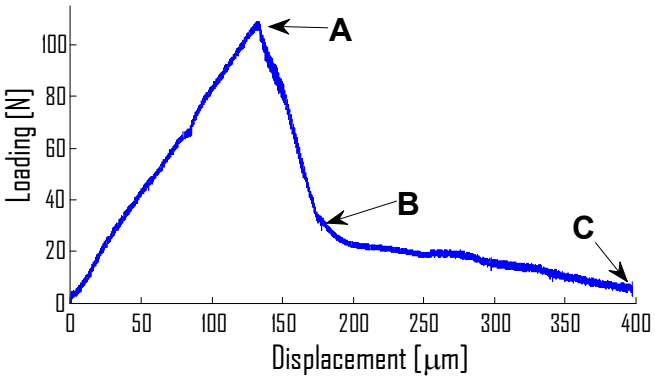

Figure 3: LD diagram. Loading levels in which FPZ zone was detailed studied are labelled by letters.

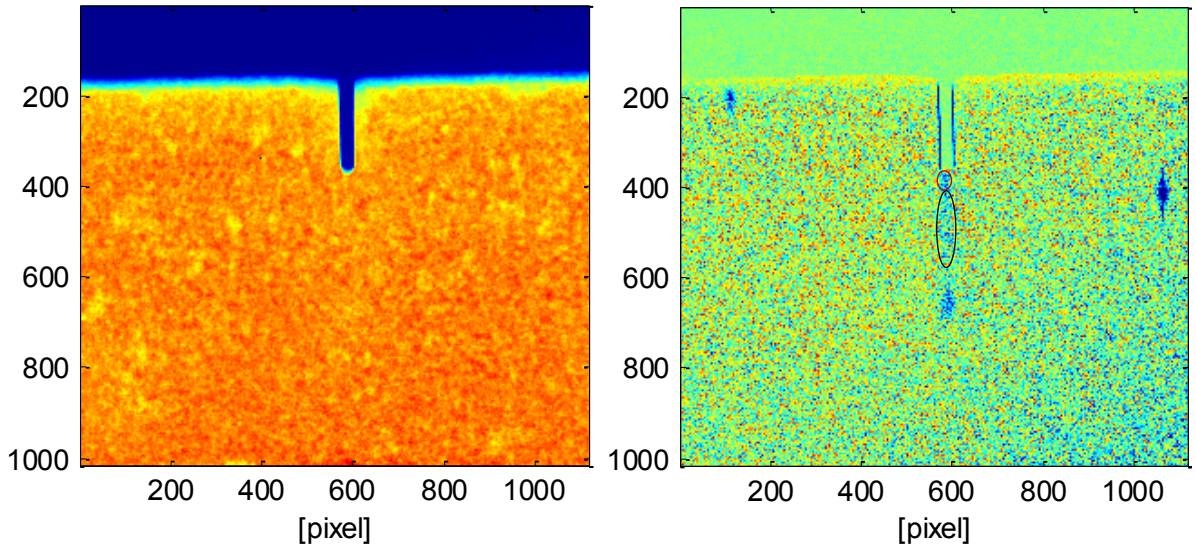

Figure 4: Radiogram of the specimen taken at the maximal loading force is left. Note, that FPZ is not visible due to significant variation of the material density. Colours correspond to the material effective density (averaged through the specimen thickness). The crack (surrounded by red ellipse) and FPZ (surrounded by black ellipse) are visible in subtraction image right. The radiogram pixel size is 44 μm.

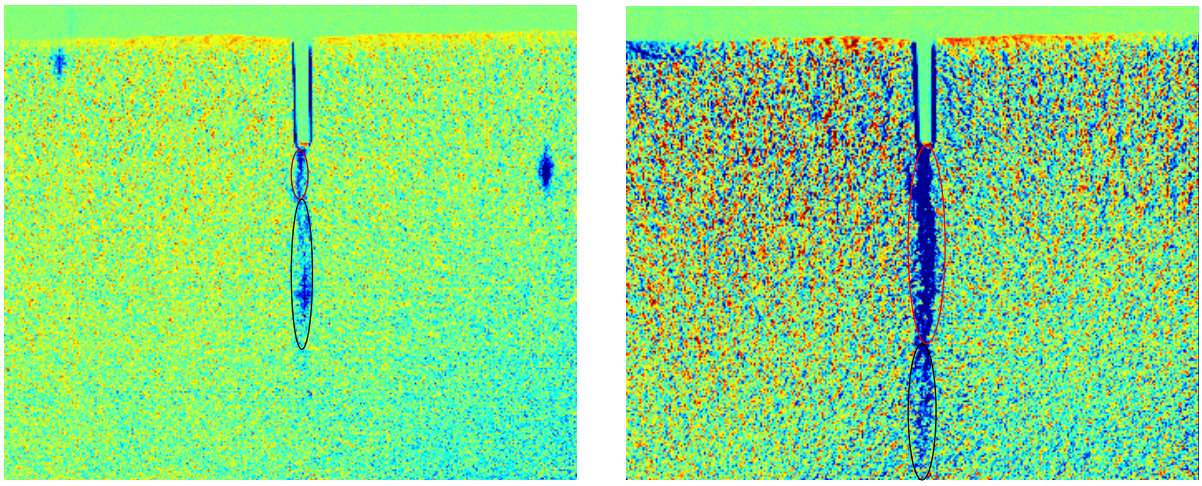

Figure 5: Subtraction image at the loading level B left. Image of the specimen at the end of the experiment is right.

The subtraction image in the moment where loading force dropped down is depicted in Figure 5 left (point *B* in LD diagram: 28 N at 160 μm). The CT measurement was done at the same loading level. It was proven that subtraction image (comparing with CT measurement) can describe crack front

position and FPZ shape thanks to the significant change of the specimen density, although boundary between crack tip and FPZ is quite blurred. Crack and FPZ were 2.7 and 16 mm long respectively at the loading level *B*. The subtraction image from the end of the loading experiment is depicted in Figure 5 right (point 3 in LD diagram: 5 N at 380 μm). The crack was 17 mm long and practically whole remaining ligament was weakened by the FPZ.

As was mentioned above, CT measurement was done in two loading levels (*B* and *C* at LD diagram). Vertical cross-section of the CT reconstruction at loading level *B* is depicted in Figure 6 left. This cross-section lies in the centre of the notch. It is visible, that specimen is damaged preferentially in the specimen centre. Virtual hole in the middle came from the flat panel local noise. Tip of transversal crack is imaged in Figure 7 right (slice number 73 at cross-section left, crack is surrounded by blue ellipse). This crack tip is in the same position as in subtraction image, Figure 5 left.

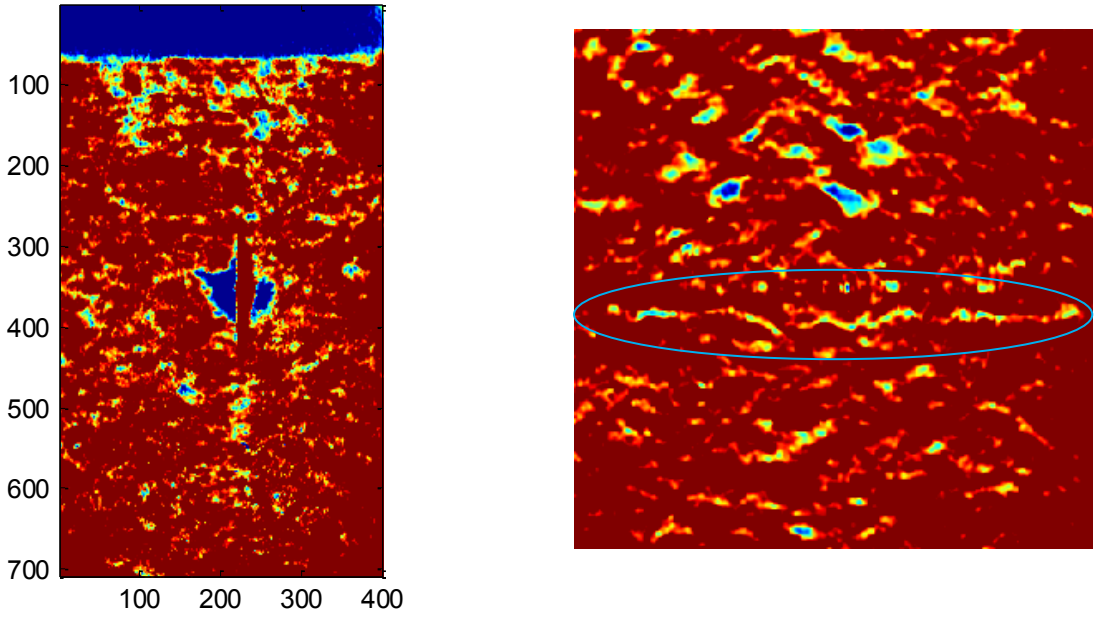

Figure 6: CT reconstruction of the specimen at loading level B. Vertical CT cross-section which corresponds to the notch central plane is imaged left. Tip of transversal crack surrounded by blue ellipse right.

Similarly, vertical cross-section at loading level *C* is imaged in Figure 7 left. Squiggly macroscopic crack from slice number 270 is in Figure 7 right.

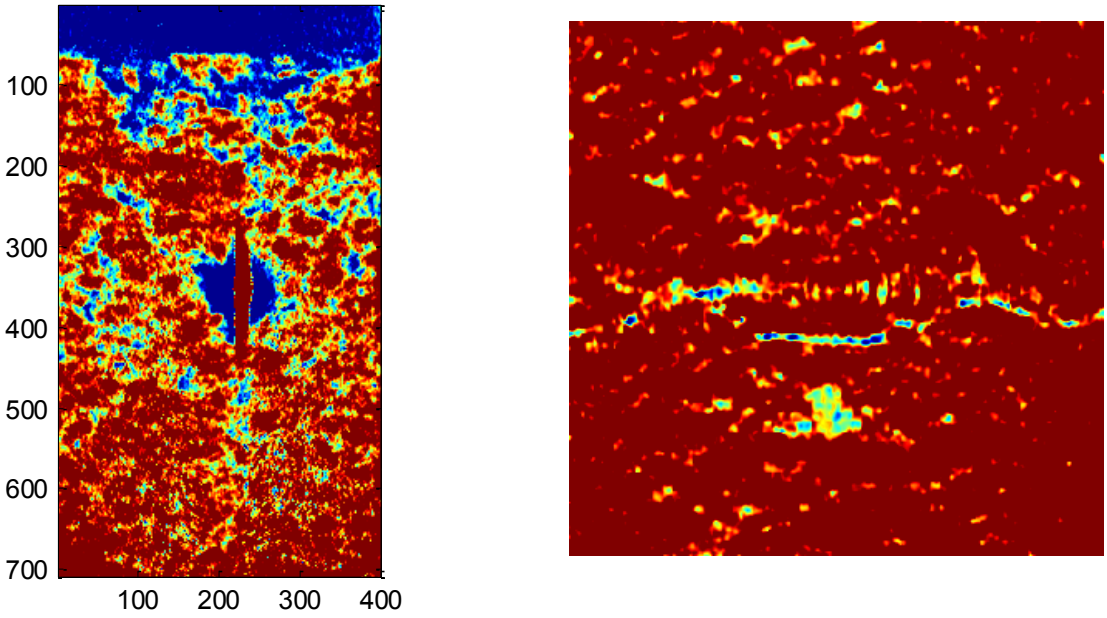

Figure 7: CT reconstruction of the specimen at loading level C. Vertical CT cross-section left. Squiggly macroscopic crack right.

Generally, crack does not follow straight direction and its front is not sharp as it is possible to document using CT reconstruction. It is hard to distinguish which individual voids were born during loading and which were presented from the beginning. However it can be shown, that void density is significantly increasing during loading as presented in Figure 8 using 3D visualization. Situation at loading *B* is left and at loading *C* right. Only central part of the specimen containing crack was selected for this visualisation.

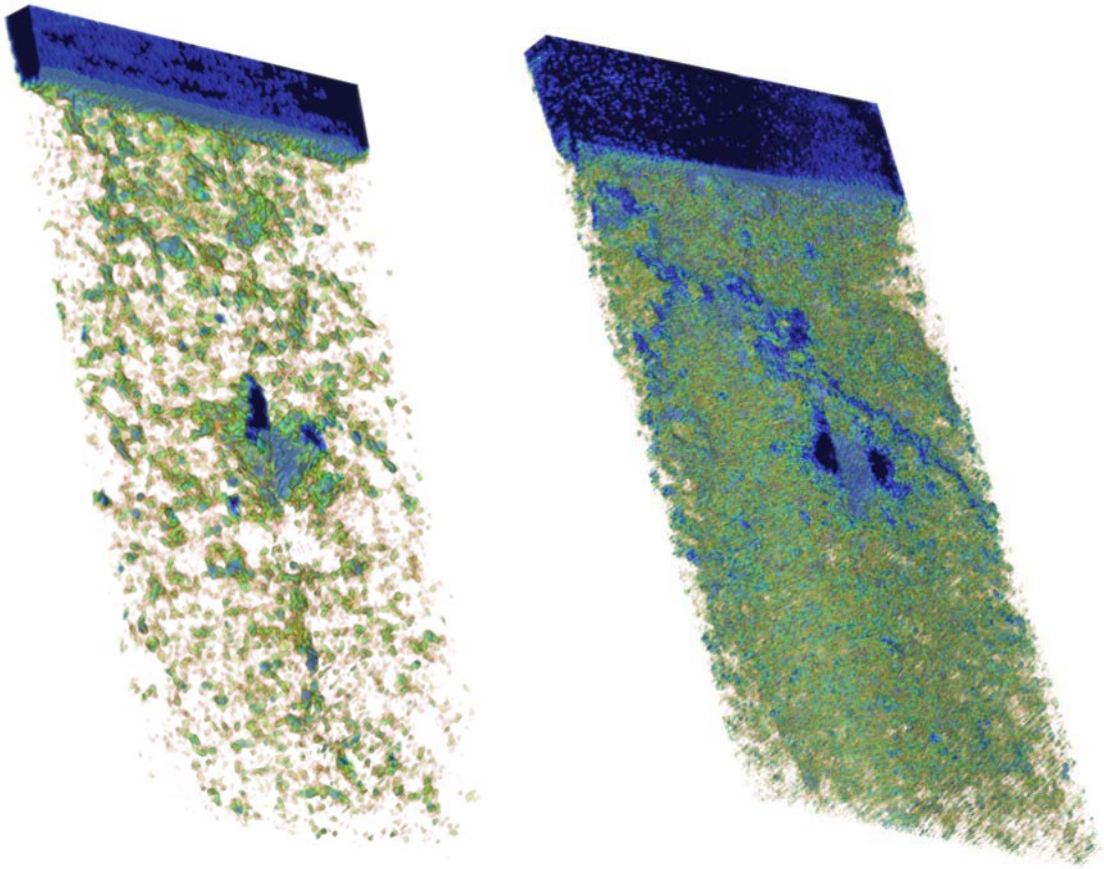

Figure 8: 3D visualisation of the voids at loading level B left and C right. It is visible that these voids and consequent macroscopic crack are preferentially occurring in the middle of the specimen.

6. Conclusions

It was proven that X-ray radiography in conjunction with Digital Image Correlation and CT reconstruction are powerful tools for analysing of the crack and FPZ evolution during quasi brittle specimen loading.

Experimental results showed that fracture process zone is generally significantly larger than macroscopic crack. Moreover, crack does not follow straight direction and its front is not sharp. It can be concluded from these reasons that linear fracture mechanics based on assumption of the continuum material can't describe such crack behaviour.

Acknowledgement

Financial support from the Czech Science Foundation, project No. P105/11/1551, and RVO 68378297 are gratefully acknowledged. Material for the specimen preparation was granted by PROFI am BAU CM, spol. s r.o.

References

Bažant, Z.P., Planas, J. (1998) Fracture and size effect in concrete and other quasi-brittle materials, CRC Press, Boca Raton.

Frantík, P., Veselý, V., Keršner, Z. (2011) Efficient lattice modelling of fracture process zone extent in cementitious composites. Proc. of the 2nd Int. Conf. on Parallel, Distributed, Grid and Cloud Computing for Engineering, P. Iványi and B.H.V. Topping (eds), Civil-Comp Press, Stirlingshire, UK, paper 62, 2011. doi:10.4203/ccp.95.62.

Hu, X-Z, Duan, K. (2007) Size effect: Influence of proximity of fracture process zone to specimen boundary. Engng. Fract. Mech. 74, 1093-1100.

Mihashi, H., Nomura, N. (1996) Correlation between characteristics of fracture process zone and tension-softening properties of concrete. Nuclear Engineering and Design 165, 359-376.

Muralidhara, S., Raghu Prasad, B.K., Eskadri, H., Karihaloo, B.L. (2010) Fracture process zone size and true fracture energy of concrete using acoustic emission. Construction and Building Materials 24, 479-486.

Otsuka, K., Date, H. (2000) Fracture process zone in concrete tension specimen. Engrg. Fract. Mech. 65, 111-131.

van Mier, J.G.M. (2007) Fracture processes of concrete: Assessment of material parameters for fracture models, CRC Press, Inc., Boca Raton.

Veselý, V, Frantík, P. (2010) Reconstruction of a fracture process zone during tensile failure of quasi-brittle materials. Applied and Computational Mechanics 4, 237-250.

Veselý, V., Frantík, P., Keršner, Z. (2009) Cracked volume specified work of fracture. Proc. of conf. CC 2009, Funchal, Portugal. B.H.V. Topping, L.F. Costa Neves, R.C. Barros (eds.), Civil-Comp Press, Stirlingshire, UK, paper 194 (16 p.), 2009. doi:10.4203/ccp.91.194.

Veselý, V., Keršner, Z., Němeček, J., Frantík, P., Řoutil, L., Kucharczyková, B. (2010) Estimation of fracture process zone extent in cementitious composites, Chem. Listy 104, 382-385.

Yu, Q., Le, J.-L., Hoover, C.G., Bažant, Z.P. (2010) Problems with Hu-Duan Boundary effect model and its comparison to size-shape effect law for quasi-brittle fracture. Journal of Engineering Mechanics (ASCE), 136(1).

Jandejsek, I., Nachtrab, F., Uhlmann, N., Vavřík, D. (2011) X-ray dynamic defectoscopy utilizing digital image correlation. Nuclear Instruments & Methods in Physics Research Section A, Vol. 6, 185-186. doi:10.1016/j.nima.2010.06.162,

Jakůbek, J., Vavřík, D., Holý, T., Jakúbek, M., Vykydal, Z., (2006), Experimental system for high resolution X-ray transmission radiography, NIM A, Vol. 563, Issue 1, p. 278-281, doi:10.1016/j.nima.2006.01.033

Vavřík, D. (2011), CT Artefact Reduction by Signal to Thickness Calibration Function Shaping, NIM A, Volume 633, Supplement 1, May 2011, Pages S152-S155, doi: 10.1016/j.nima.2010.06.160

Vavřík, D., Soukup, P. (2011) Metal Grain Structure Resolved with Table-top micro-Tomographic System, JINST_007P_1011, doi:10.1088/1748-0221/6/11/C11034